Adams, M.; Kozlowska, M.; Baroni, N.; Oldenburg, M.; Ma, R.; Busko, D.; Turshatov, A.; Emandi, G.; Senge, M. O.; Haldar, R.; Wöll, C.; Nienhaus, G. U., Richards, B. S.; Howard, I. A. (2019):
Highly Efficient One-Dimensional Triplet Exciton Transport in a Palladium–Porphyrin-Based Surface-Anchored Metal–Organic Framework.
ACS Applied Materials & Interfaces 11, 15688–15697. doi: 10.1021/acsami.9b03079

Highly efficient 1D triplet exciton transport in a palladium-porphyrin based surface-anchored metal-organic framework

Michael Adams[1], Mariana Kozlowska[2], Nicolò Baroni[1], Michael Oldenburg[1], Rui Ma[3], Dmitry Busko[1], Andrey Turshatov[1], Ganapathi Emandi[4], Mathias O. Senge[4], Ritesh Haldar[5], Christof Wöll[5], G. Ulrich Nienhaus[2,3,6,7], Bryce S. Richards[1,8], Ian A. Howard[1,8,]*

[1] Institute of Microstructure Technology, Karlsruhe Institute of Technology, Herrmann-von-Helmholtz-Platz 1, 76344 Eggenstein-Leopoldshafen, Germany

[2] Institute for Nanotechnology, Karlsruhe Institute of Technology, Herrmann-von-Helmholtz-Platz 1, 76344 Eggenstein-Leopoldshafen, Germany

[3] Institute of Applied Physics, Karlsruhe Institute of Technology, Wolfgang-Gaede-Straße 1, 76131 Karlsruhe, Germany

[4] School of Chemistry, SFI Tetrapyrrole Laboratory, Trinity Biomedical Sciences Institute, Trinity College Dublin, The University of Dublin, 152-160 Pearse Street, Dublin, Ireland

[5] Institute of Functional Interfaces, Karlsruhe Institute of Technology, Herrmann-von-Helmholtz-Platz 1, 76344 Eggenstein-Leopoldshafen, Germany.

[6] Institute of Toxicology and Genetics, Karlsruhe Institute of Technology, Herrmann-von-Helmholtz-Platz 1, 76344, Eggenstein-Leopoldshafen, Germany.

[7] Department of Physics, University of Illinois at Urbana-Champaign, 1110 West Green Street, Urbana, IL, U.S.A.

[8] Light Technology Institute, Karlsruhe Institute of Technology, Wolfgang-Gaede-Straße 1, 76131 Karlsruhe, Germany.

[*] Corresponding author: ian.howard@kit.edu

KEYWORDS

exciton transport, metal-organic frameworks, porphyrin, thin films, transient absorption, electronic coupling, DFT

ABSTRACT

Efficient photon harvesting materials require easy-to-deposit materials exhibiting good absorption and excited-state transport properties. We demonstrate an organic thin-film material system, a palladium-porphyrin based surface-anchored metal-organic framework (SURMOF) thin film, that meets these requirements. Systematic investigations using transient absorption spectroscopy confirm that triplets are very mobile within single crystalline domains; a detailed analysis reveals a triplet transfer rate on the order of 10^{10} s^{-1}. The crystalline nature of the SURMOFs also allows a thorough theoretical analysis using density functional theory (DFT). The theoretical results reveal that the intermolecular exciton transfer can be described by a Dexter electron exchange mechanism that is considerably enhanced by virtual charge-transfer exciton intermediates. Based on the photophysical results, we predict exciton diffusion lengths on the order of several micrometers in perfectly ordered, single-crystalline SURMOFs. In the presently available samples, strong interactions of excitons with domain boundaries present in these metal-organic thin films limit the diffusion length to the diameter of these two-dimensional grains, which amount to about 100 nm. These results demonstrate potential of SURMOFs for energy harvesting applications.

TEXT

1. Introduction

Originally designed for gas storage and separation,[1] metal-organic frameworks (MOFs) have started to create an impact as designer materials for electric, electronic and optical properties.[2] Since the discovery that the ionic[3] and electrical[4] conductivity of these materials can be tuned over many orders of magnitude, their prospect to exhibit novel features has stirred a huge interest, also with regard to photophysical properties, such as light-harvesting,[5,6] photovoltaics,[7] photocatalysis,[8] and even solar-powered water harvesting from air.[9] Of particular interest in this context is the mobility of the excited states, such as charges or excitons, which affects the efficiency of the material's transport properties and, in organic materials, is directly linked to the degree of molecular long-range order.[10] Therefore, crystalline MOFs can be expected to have an inherent advantage over less ordered organic semi-conducting systems such as polymers.

Outside the realm of MOFs, there exist already numerous promising organic materials with excellent transport properties, such as singlet exciton transport over distances on the micron scale due to coherent effects (for example self-assembled organic systems such as nanotubes[11], nanofibers,[12] and in a conjugated polymer wire embedded in a crystal[13]), or triplet exciton transport over 4 μm in an organic crystal.[14] However, these materials share a drawback: in their current state, they are difficult to mass-fabricate or deposit on large surface areas, as would be necessary for applications outside the laboratory. In contrast, surface-anchored metal-organic frameworks (SURMOFs) – thin MOF films attached to a substrate – can be fabricated in a fast and easy way from solution.[15] SURMOFs exhibit crystalline order, making them promising

candidates for outstanding transport properties. Indeed, singlet transport in MOFs and SURMOFs has been a topic of significant, and ongoing investigation.[16–24] The knowledge of atomic positions assists in this respect by providing the basis for a thorough theoretical analysis.[16,17,25] Additionally, SURMOF film thickness is tunable from tens to hundreds of nanometers, and the films have excellent optical quality (as illustrated in Figure 1a).

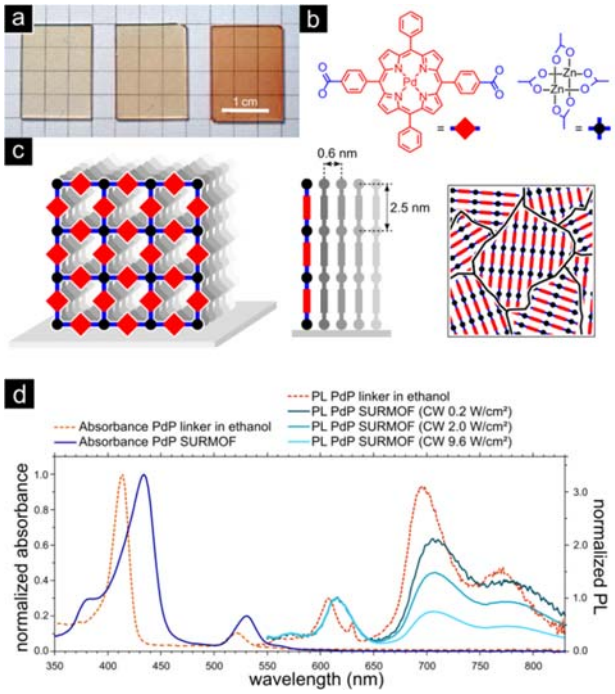

Figure 1. PdP SURMOF. (**a**): Photograph of three PdP SURMOF thin film samples on glass substrates fabricated with increasing number of spraying cycles (from top to bottom: 2, 4 and 15 cycles). **(b)** Chemical structure of the PdP linker molecule and the zinc paddlewheel metal center. (**c**): Schematic drawing of the PdP SURMOF showing the arrangement of the linker and metal center into sheets that stand on the substrate and form randomly oriented crystalline domains in the plane of the substrate. **(d)** Absorbance and steady-state PL spectra of the PdP linker in ethanol and of a PdP SURMOF. The PL spectra are normalized to the fluorescence peak around 610 nm. The bands at 700 nm and 800 nm are the phosphorescence. The ratio of fluorescence to phosphorescence is increased in the SURMOF due to a suppression of the phosphorescence caused by triplet-triplet annihilation for excitation power densities of 0.1 W/cm² and above.

As opposed to singlet transport, there is no theoretical upper bound to the length of triplet diffusion.[26] Furthermore, triplet exciton transport is a Dexter rather than a Förster process, which was suggested to be advantageous for solar energy harvesting materials, especially in combination with one-dimensional (1D) transport.[27] For this reason, we systematically investigate the triplet excited-state transport properties of a previously established type of SURMOF based on palladium-porphyrin linker molecules (depicted in Figures 1b and 1c). To date, the material's photovoltaic activity was demonstrated,[7] it was successfully used as a sensitizing layer in a photon upconversion system,[28] and, recently, its photostability was examined.[29] However, no systematic investigation of the excited-state transport in this material has been performed yet. Here, we report highly efficient triplet excited exciton transport in a palladium-porphyrin SURMOF thin film material with a triplet transfer rate on the order of 10^{10} s^{-1}, which yields a theoretical diffusion length of several microns. We analyze in detail the origin of these unexpectedly large transfer rates and discuss the current limitations in experimentally reaching the theoretically predicted diffusion lengths.

2. Results and discussion

2.1 Sample characterization

The SURMOF material used in the current study is based on the established SURMOF-2 structure[7,29,30] and is fabricated using a spraying technique:[31] Zn paddlewheel nodes are coordinated to four ditopic organic linkers (5,15-bis(4-carboxyphenyl)-10,20-

diphenylporphyrinato)palladium(II) (PdP), as shown in Figure 1. This method yields an assembly of planar sheets with four-fold symmetry, in which the metal centers and linkers are held together by strong carboxylate-metal ion bonds. Previous structural characterization revealed that the length of a unit cell within a sheet is 2.5 nm (primarily determined by the length of the PdP linker molecule, see also Figures S14 and S15 for experimental XRD data), while the distance between two sheets is 0.6 nm.[7] The SURMOF structure is stable under vacuum conditions as used in our experiments (see Supporting Information for details). As discussed below, this small inter-sheet distance leads to a preference of one-dimensional (1D) exciton transport in between the SURMOF sheets as opposed to transport inside the sheets. This 1D exciton motion is facilitated by the highly π-delocalized nature of the PdP linker molecules and their π-orbital overlap in the short-distance inter-sheet direction.[32]

The PdP linker molecule exhibits a high intersystem-crossing rate due to spin-orbit coupling induced by the metal center, leading the initially-created singlet excitons to transform into a triplet-exciton population with an efficiency close to unity.[33] The spin-orbit coupling allows radiative decay from the triplet excited state, leading to strong phosphorescence (see Figure 1d). The ratio between fluorescence and phosphorescence intensity strongly depends on the excitation fluence. As the singlet exciton lifetime remains very short in the PdP SURMOF (less than 20 ps)[7], this change in ratio cannot be ascribed to an increase of the fluorescence in the SURMOF. Instead, it is indicative of efficient triplet-triplet annihilation, which is discussed further below. The intrinsic lifetime of the triplet state in the PdP SURMOF is established as $\tau = (729 \pm 2)$ μs (see Figure S1), measured after low-fluence excitation. This is longer than the triplet lifetime of a reference compound, PdTPP [5,10,15,20-tetrakis(4-phenylethynyl)phenylporphyrinato)palladium(II)] dissolved in toluene.[34] The extended triplet

lifetime in the SURMOF indicates a suppression of non-radiative decay pathways. The rigidifying effect of the SURMOF structure and the reduction of surrounding solvent molecules can both contribute to this suppression.

The absorbance of the PdP linker in ethanol solution (Figure 1d) is characterized by the Soret band at 415 nm and the maximum Q-band absorption at 520 nm. In the SURMOF, the maximum of the Soret band absorption is red-shifted by 0.138 eV to 435 nm and the absorption band is significantly broadened. The Q-band absorption maximum is also slightly red-shifted (to 530 nm) in the SURMOF, with the photoluminescence redshifting by a similar amount. The significant bathochromic shift is caused by stacking of the PdP linkers in the SURMOF, leading to the formation of aggregates.[32,35] The close packing of neighboring PdP molecules (see Figure 2a) induces strong π-π intermolecular interactions between the highly aromatic porphyrin fragments. These noncovalent interactions as obtained by quantum-chemical calculations are depicted in Figure 2b. They are found to be very dense and spread over the entire PdP fragment, leading to a high intermolecular binding energy of 1.34 eV in the SURMOF between PdP molecules on adjacent sheets (estimated using a supermolecular approach, see Supporting Information). These strong and delocalized π-π interactions affect the electron density localization on the PdP frontier orbitals (see Figure S12) and lead to a shift in their energy difference, which leads to bathochromic shifts in the various optical transitions (although we note that the size of the shifts to the different transitions vary because of the varying relative contributions of the different frontier orbitals for different transitions).

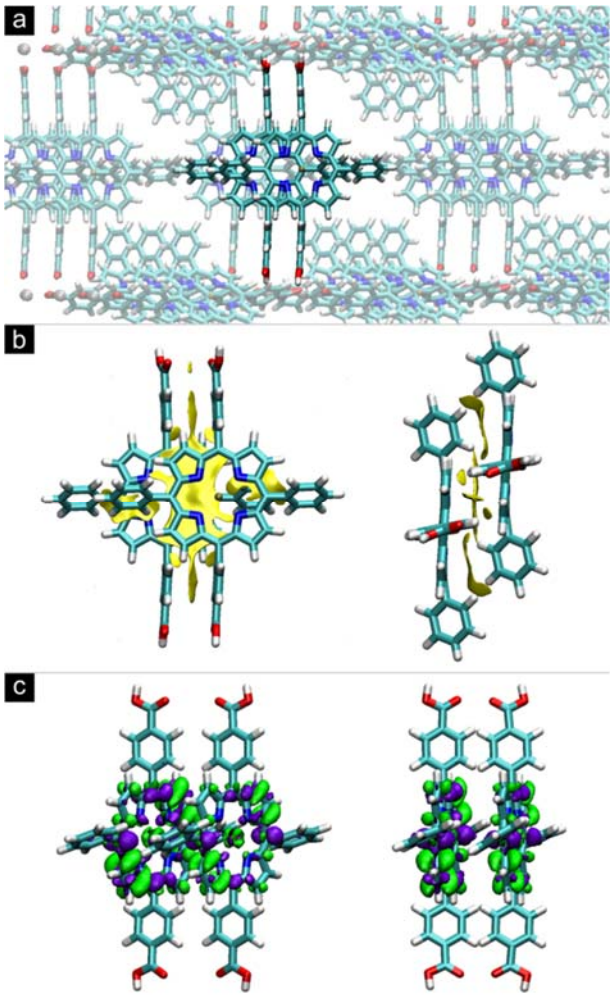

Figure 2. (a) 3D visualization of the arrangement of PdP chromophores in the ground-state optimized structure of the SURMOF (three sheets shown, a dimer as used for the simulations is highlighted). **(b)** π-π-interactions in a PdP SURMOF. Visualization of intermolecular noncovalent interactions (NCI) between neighboring PdP linkers in SURMOF (in yellow). The depicted NCI surface corresponds to the reduced density gradient of 0.4 a.u.[36] A description of the theoretical methods used is given in Supporting Information. **(c)** Visualization of the electron density difference between the ground and triplet excited states of the PdP dimer, obtained using TD-DFT calculations with CAM-B3LYP functional (see Supporting Information). The electron-donating and electron- accepting regions are marked in violet and green, respectively (isovalue of 3×10^{-4} a.u.).

2.2 Transient absorption spectroscopy

In order to experimentally investigate the exciton transport in a PdP SURMOF, we performed nanosecond transient absorption spectroscopy (TAS). The spectra recorded at different delay times (see Figure 3a) can be described by the decay of a single spectrum, which is dominated by a broad photo-induced absorption (PIA, $\Delta OD>0$) of an excited state, and has a maximum between 450 and 500 nm. The dip in the spectrum at the pump wavelength 532 nm can be attributed to a small contribution of a ground state bleach signal (GSB, $\Delta OD<0$). The sum of these two contributions makes up the spectra and their relative weight does not change, the spectra at each time delay retain their shape and only change in scale, thus confirming that only a single long-lived excited-state species is created after photoexcitation of the PdP SURMOF. These long-lived species are the triplet excitons responsible for the phosphorescence in the PL measurements discussed above.

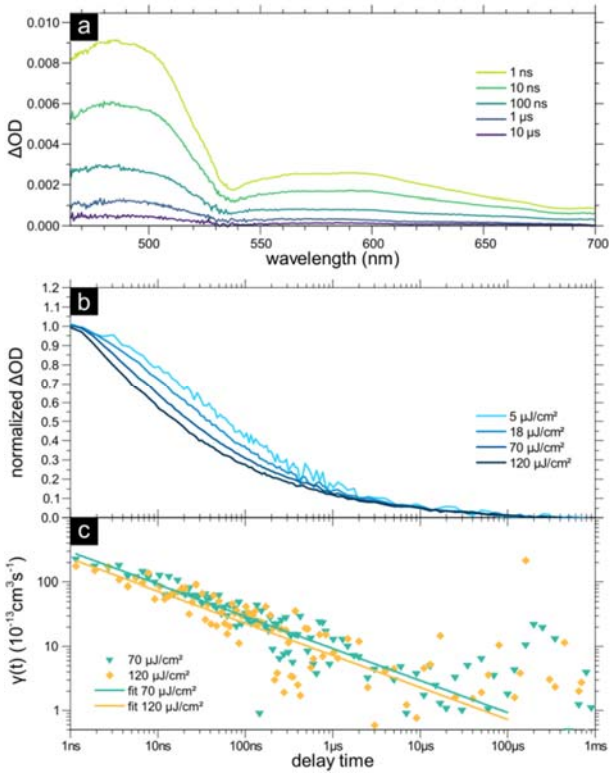

Figure 3. Transient absorption spectroscopy (TAS). Transient absorption data for a PdP SURMOF thin film sample excited at 532 nm under dynamic vacuum (<10^{-4} Pa). **(a)** TAS spectra (change in optical density ΔOD) at specific delay times (excitation fluence 70 µJ/cm^2). (**b**) Normalized TAS kinetic traces for different excitation fluences. (**c**) TTA rate coefficient $\gamma(t)$ for the highest two excitation fluences calculated from the data in (b) as described in the text. The solid lines represent fits with a 1D diffusion model.

We examine the triplet exciton population kinetics in the PdP SURMOF by comparing the TAS kinetics for a series of different excitation fluences (see Figure 3b), using the TAS signal integrated in the 460-500 nm wavelength region (selected for its high signal strength). As the initial excited-state density in the sample is raised by increasing the excitation fluence, the decay of the triplet population becomes faster. This indicates the presence of triplet-triplet interactions and we attribute the population decrease to triplet-triplet annihilation (TTA). This

process requires two triplets to meet, with the collision rate increasing with triplet density and triplet mobility. Thus, the decay rate of the triplet population becomes faster as the excitation fluence is increased. For a detailed discussion of how TTA is the dominant deactivation channel at these fluences (meaning the vast majority of the triplet population is mobile and able to participate in this TTA process) please see the Supporting Information. In particular, the change in the triplet kinetics is not caused by temperature changes in the SURMOF, as laser-induced heating is negligible here (see Supporting Information).

The fact that no decay component on the order of the monomolecular lifetime can be observed in Figure 3b highlights the good connectivity of the SURMOF: The bulk of the PdP molecules are well-connected, enabling triplet exciton transport and TTA. No contribution of isolated, monomer-like molecules (e.g. at the SURMOF's surface) can be observed, as they would result in immobile triplet excitons decaying with their monomolecular lifetime. Given the signal-to-noise ratio of the TAS data, the percentage of such isolated PdP chromophores can be estimated roughly as <5%.

The total decay of the triplet exciton population can be described by a single rate equation:

$$\frac{dT}{dt} = -k_{\mathrm{T}\rightarrow\mathrm{GS}}T - f\gamma(t)T^2 \ , \qquad (1)$$

where T denotes the concentration of the triplet exciton species, $k_{\mathrm{T}\rightarrow\mathrm{GS}}$ is the rate of triplet decay to the ground state *via* monomolecular (radiative and non-radiative) channels, f is a factor that depends on the expectation value for the number of triplets remaining after a triplet-

triplet encounter (here f = 1, see the Supplementary Material) and $\gamma(t)$ denotes the time-dependent TTA rate constant.

The time dependence of the rate of triplet-triplet annihilation is linked to the dimensionality of the diffusion process, for example for one-dimensional (1D) diffusion $\gamma(t) \propto \sqrt{D/t}$,[37] whereas in the 3D case $\gamma(t)$ tends to a constant at longer times.

From Equation 1 we can derive the following expression for the TTA rate:

$$\gamma(t) = T(t)^{-2} \left(\frac{dT(t)}{dt}\right). \quad (2)$$

Here we simplified the equation by neglecting the linear term using the assumption that $k_{\mathrm{T}\rightarrow\mathrm{GS}} T \ll \gamma T^2$, which is valid at early times for high excitation fluences as under such conditions TTA is the predominant decay channel.

The necessary values of the triplet concentration $T(t)$ can be derived from the TAS kinetics with the knowledge of the initial concentration T^0 (see Supplementary Material). Using this experimentally determined $T(t)$ and its numerically calculated first derivative, we translate the TAS kinetics into the experimental values for $\gamma(t)$, as shown in Figure 3c. The data at the two highest excitation fluences were used because they have the best signal-to-noise ratio and, therefore, are preferable for numerical calculation of the first derivative. A similar value of $\gamma(t)$ is obtained for both fluences, corroborating our assumption that under these experimental conditions, the bimolecular triplet annihilation is much faster than the monomolecular decay. The value of $\gamma(t)$ decreases monotonically over time, which is consistent with the expected functional behavior of $\gamma(t)$ for one-dimensional diffusion. This can be seen from the fits using

$\gamma(t) = \gamma_0 t^{-1/2}$, which describe the data well. The value for the constant γ_0 from concurrently fitting both data sets is $\gamma_0 = (8.2 \pm 0.2) \times 10^{-16}\mathrm{cm}^3\mathrm{s}^{-1/2}$. We note that our data is inconsistent with the 3D function for $\gamma(t)$ (see Figure S4). From this, we can conclude that the triplet exciton transport is primarily 1D within the SURMOF.

We note that this strong evidence for 1D exciton motion in between the porphyrin layers is consistent with reports on anisotropic photoconductivity in porphyrin single-crystals,[38] singlet transport in a Zn-porphyrin MOF,[17] and anisotropic exciton diffusion in SURMOFs made from anthracene dibenzoic acid.[23]

With γ_0 we calculate the diffusion coefficient D using the relation[39]

$$\gamma(t) = \frac{1}{a \cdot n}\sqrt{\frac{8D}{\pi t}} = \gamma_0 \frac{1}{\sqrt{t}}, \qquad (3)$$

where a is the distance between molecules along the transport dimension (in our case a=0.6 nm) and n is the 3D concentration of molecules in the sample (from the unit cell depicted in Figure 1 we calculate n=2×(2.5 nm×2.5 nm×0.6 nm)$^{-1}$=5.33×10^{20}cm^{-3}). Solving for D yields a diffusion coefficient of (2.7±0.4)×10^{-4} cm^{2}s^{-1} , with the uncertainty being calculated from the fitting uncertainty of γ_0 and conservatively assuming uncertainty in the unit cell dimensions of 0.1 nm. An additional source of uncertainty comes from our use of the thin film approximation for the calculation of the initial triplet concentration T^0 (see Supporting Information), which results in lower and upper boundaries on D of 1.6×10^{-4} cm^{2}s^{-1} and 5.5×10^{-4} cm^{2}s^{-1} (assuming a ±30% error in T^0 due to the approximation). The triplet exciton hopping rate k_{hop} in ordered 1D systems can be expressed in terms of the diffusion coefficient:[40]

$$k_{\text{hop}} = \frac{D}{a^2}, \quad (4)$$

and we find k_{hop}=8×10^{10} s^{-1} for the triplet exciton energy transfer (TEET) in PdP SURMOFs (with uncertainty boundaries as discussed above of 4.7×10^{10} s^{-1} and 16.3×10^{10} s^{-1}). Although this value is significantly higher than TEET rates in (disordered) conjugated polymers (10^{6} s^{-1}),[41] it is similar to TEET rates in tetracyanoquinodimethane (TCNQ) salts (10^{7} s^{-1} - 10^{11} s^{-1}),[42] tetracene crystals (10^{10} s^{-1} - 10^{11} s^{-1}),[43] or triisopropylsilylethynyl acetylene (TIPS) pentacene thin films (10^{11} s^{-1}).[44] In the realm of MOFs, the 1D TEET rate in a Ru-trisbipyridyl-based system (with chromophore separation distances of >0.8 nm) was reported to be on the order of 10^{8} s^{-1}.[27]Förster transport of singlet excitons was found to be faster in two different Zn-porphyrin MOFs (10^{12} s^{-1} - 10^{13} s^{-1}),[17,21] whereas our hoping rate is similar to the electron transfer rate in a pyrene based MOF (10^{10} s^{-1}).[45] These comparisons show that the PdP SURMOF TEET rate is competitive with respect to other material systems while offering its own advantages, namely in the ease of fabrication of thin films and the 1D nature of the transport.

2.3 Quantum mechanical calculations

In order to demonstrate the 1D nature of the exciton transport in PdP SURMOFs, we performed quantum mechanical calculations using density functional theory (DFT) and time-dependent DFT, as described in the Supplementary Material. The diffusion of triplet excitons, which are the main long-lived excited-states in the PdP SURMOF, is described by a short-ranged intermolecular exciton transfer process. Owing to the fact that excitons in MOF systems are well localized on single linker molecules that are separated by much larger distances than typical for organic crystals, they are characterized by the weak electronic coupling regime[46] In such

conditions, the triplet excited exciton transfer rate, k_{TEET}, can be calculated by Fermi's golden rule as:

$$k_{\mathrm{TEET}} = \frac{2\pi}{\hbar}|V_{\mathrm{TEET}}|^2(\mathrm{FCWD}), \quad (5)$$

where $\hbar$ and V_{TEET} denote Planck's constant divided by 2π and the electronic coupling matrix element between adjacent molecules; (FCWD) is the Franck-Condon weighted density of states, which can be calculated using classical, semi-classical or quantum-mechanical theories. In the present work, we use the semi-classical Marcus theory expression,[47,48] to estimate the theoretical TEET transfer rates for the PdP SURMOF. The standard Gibbs free energy change vanishes in absence of an electric field for systems wherein donor and acceptor molecules are identical. Therefore, the resulting transfer rate is:

$$k_{TEET} = \frac{2\pi}{\hbar}|V_{\mathrm{TEET}}|^2\sqrt{\frac{1}{4\pi k_B T\lambda}}\exp\left(-\frac{\lambda}{4k_B T}\right), \quad (6)$$

where V_{TEET} is the electronic coupling matrix element between the initial state of a donor and the final state of the acceptor during the exciton transfer. This corresponds to an exciton moving between two adjacent sites in the SURMOF. λ is the reorganization energy, connected to the change in equilibrium geometry of both donor and acceptor upon TEET.

The electronic coupling element, V_{TEET}, is determined by the nature of the electronic wavefunctions of the molecules involved in the energy transfer. An important component to V_{TEET} is the simultaneous exchange of an electron in the highest occupied molecular orbital (HOMO) and the lowest unoccupied molecular orbital (LUMO) between a donor and an acceptor molecules, known as Dexter electron exchange transfer.[49] It was shown recently that V_{TEET}

cannot be explained by the Dexter mechanism alone.[50–52] The contribution of the electron density overlap,[50,51] and virtual charge transfer exciton intermediates[50,51,53,54] can be strong and enhance the transfer rate. Especially the last term is of significant importance in the sequential type pathway of the Dexter energy transfer,[53,54] when the exciton moves not as an entity, but through sequential hops of a LUMO electron and an HOMO hole, creating intermediate charge transfer (CT) configurations described by new donor and acceptor wave functions. Wehner *et al.* have shown that for TEET in pyrene molecules, the addition of CT exciton intermediates for HOMO and LUMO transfers results in a significant improvement of the TEET coupling.[54]

Therefore, we use the TEET electronic coupling elements with included overlap integrals[50–52] and CT configurations for the frontier orbitals[55] to estimate the triplet exciton transfer rate k_{TEET} for adjacent molecules along the 1D pathways in the PdP SURMOF. The calculated electronic coupling elements and the transfer rates are listed in Table 1. The transfer rates were calculated using equation 6 (with λ = 0.256 eV, approximated as the inner reorganization energy contribution, see Supporting Information).

Table 1. Electronic coupling matrix elements (V) and corresponding transfer rates (k) for the Dexter exchange, electron density overlap, triplet excited exciton transfer (TEET) and virtual charge transfer (CT) exciton intermediates for the PdP linkers in the SURMOF. The values were obtained using the energy splitting method[56] for the PdP dimer utilizing DFT and TD-DFT calculations with hybrid B3LYP and long-range separated CAM-B3LYP functionals, as described in the Supporting Information.

	***V* (meV)**		***k* (s^{-1})**	
	B3LYP	CAM-B3LYP	B3LYP	CAM-B3LYP
Dexter	0.036	0.099	3.67×10^6	27.8×10^6

Density overlap	0.400	0.196	-	-
TEET	0.436	0.296	5.30×10^{8}	2.43×10^{8}
CT HOMO	38.9	49.1	4.22×10^{12}	6.71×10^{12}
CT LUMO	7.21	8.84	1.45×10^{11}	2.18×10^{11}
Virtual CT	1.04	1.61	3.03×10^{9}	7.24×10^{9}
TEET+Virtual CT	1.48	1.91	0.61×10^{10}	1.01×10^{10}

We find that the calculated values for the TEET transfer rate (1.01×10^{10} s^{-1}), for short range electronic coupling elements including Dexter transfer, electronic density overlap and intermediate CT configurations, are comparable with the experimentally obtained $k_{hop}=8\times10^{10}$ s^{-1}. This confirms that the experimental data on triplet exciton diffusion in PdP SURMOFs is dominated by a sequential 1D short range electron exchange process, as visualized in Figure 2c. It is not surprising that the calculated values for k_{TEET} is somewhat smaller than the experimental results, because higher order intermediate CT excited configurations of the donor and acceptor may also contribute to the overall TEET coupling.[54] In addition, dynamic deviations of the PdP linkers in the SURMOF, such as a decrease the intermolecular distance, might also affect the electronic coupling elements and increase the exciton transfer rate.[57,58]

From the experimentally-derived diffusion coefficient, D (directly related to the hop frequency), and monomolecular lifetime, τ, we can obtain a theoretical estimate for the diffusion length L of the triplets using the relationship

$$L = \sqrt{2ZD\tau}\ ,$$

(7)

where Z is the dimensionality of the diffusion process (in our 1D system, $Z = 1$) and τ is the exciton lifetime in the absence of TTA. From Equation 4 we obtain a 1D diffusion length of L = 6.3 μm (with uncertainty boundaries of 4.8 μm and 9.0 μm, due to the thin film approximation) This is of the same order as the 3D triplet diffusion length of 1.6 μm established in an anthracene MOF (whose diffusion coefficient was determined to be on the order of 10^{-6} cm^2s^{-1}).[59] As transport is restricted to one dimension in our PdP SURMOF, for a perfect single crystal a triplet exciton has an average displacement of $L/a \approx 10^4$ porphyrin units.

2.4 Luminescence microscopy

Diffusion on the micron length scale should be directly observable with photoluminescence microscopy experiments.[11,14] To this end, an encapsulated PdP SURMOF thin film was excited at 405 nm (continuous wave, CW) and the resulting phosphorescence distribution was imaged. When comparing excitation (Figure 4a) and emission images (Figure 4b), the phosphorescence PL spot appears to be larger than the excitation spot measured by reflection from a mirror. At first sight, this broadening could be diffusion of the excited states from the sites at which they are generated into the surrounding material. However, after careful analysis and additional experimentation we find that this broadening can be completely explained by scattering of the excitation light coupled with very efficient TTA.

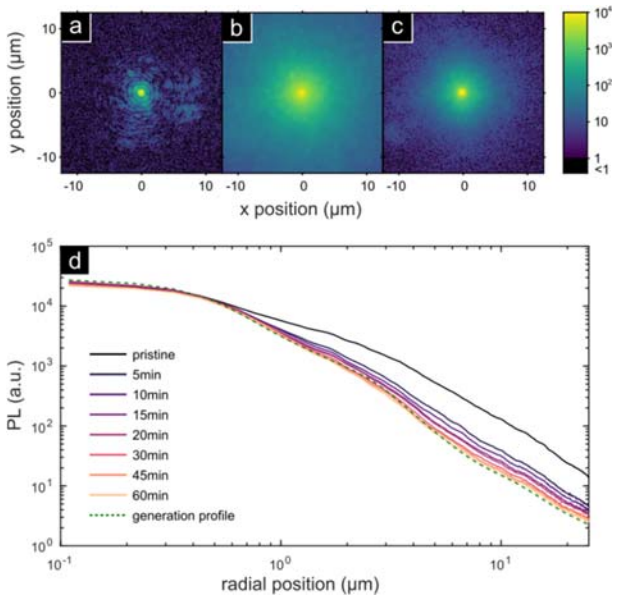

Figure 4. Phosphorescence microscopy. **(a)** Reflection intensity of the 405 nm CW excitation beam on a mirror. **(b)** Phosphorescence intensity of an encapsulated pristine PdP SURMOF thin film sample at room temperature excited at 405 nm (CW, 19.3 W/cm²). **(c)** Phosphorescence intensity of an encapsulated PdP SURMOF thin film sample at room temperature excited at 405 nm (CW, 19.3 W/cm²) after 60 minutes of illumination (405 nm CW at 1.2 W/cm² with 70 µm beam diameter). **(d)** Radial phosphorescence profile for an encapsulated PdP SURMOF thin film sample at room temperature excited at 405 nm (CW, 69.3 W/cm²) at different illumination durations. The green dashed line represents the shape of the exciton generation profile used in the simulation (see text).

To explain the observed broadening, we consider a simple model that allows generation and annihilation of the triplet density at each radial position, but no long-range diffusion. This approximates the situation wherein triplets can move efficiently within their domain (therefore allowing annihilation) but cannot move long distances due to the grain boundaries between

crystals (see Supporting Information for details on the simulation). We find that such a simple simulation can adequately describe the observed PL spot sizes for a variety of excitation fluences when a generation profile with longer "wings" as compared to the measured excitation spot is used. This weak excitation far from the center spot could be caused by scattering of the excitation spot into the film, or glass substrate, causing modes radiating from the center of the excitation spot that are gradually absorbed by the thin-film.

To further assess the feasibility of this explanation, we deliberately changed the monomolecular lifetime of the PdP molecules by introducing quenching sites. We did this by prolonged illumination of the sample to introduce quenching photoproducts.[29] As the sample is exposed to prolonged illumination, the observed PL profile decreases in width (see Figure 4c) and comes closer and closer to the excitation profile (see Figure 4d). This is because the increasing influence of the quenching pathway reduces the share of triplets that are deactivated by TTA (an extended discussion can be found in the Supporting Information). Without TTA (or diffusion), the phosphorescence profile obviously matches the generation profile. Therefore, we can refine our simulation by using the phosphorescence profile of the most-degraded sample (see Figure S8 and the green line in Figure 4d) as an empirical proxy for the generation profile.

We note that the PL intensity measured in the center of the excitation spot barely changes with degradation at all (Figure 4d). This is because at the high triplet densities present in the center of the spot the photoluminescence quantum yield (PLQY) is low even in the pristine material, so the amount of emission changes relatively little by degradation. The PLQY is either low due to dominant TTA, or due to quenching. Far from the spot center, where TTA becomes negligible, the PL-decrease with prolonged illumination is more drastic, which is reflective of the change in the monomolecular rate. We simulated the profiles for the pristine condition and at all

degradation times and find them in good agreement with the experimental data (see Figure S9 in the Supporting Information). Hence, all measured data are consistent with our explanation based on considering TTA and excluding long-range diffusion. As a side note in relation to our previous publication,[29] this simulation allows us to extract the change in the monomolecular rate k and, in turn, the heretofore unknown radical-pair generation rate k_R, which we find to be on the order of 10^4 s^{-1} after an hour of illumination.

After having demonstrated that the luminescence spots can be explained by scattering effects and TTA, we turn our attention to the question why the large theoretical diffusion length does not yield a more pronounced broadening of the profiles. We feel that the only possibility to explain this observation is to consider the effect of domain boundaries within the SURMOFs. While all domains are oriented with their (001) crystallographic direction normal to the substrate, the orientation of this direction is different for each crystal domain (see Figure 1c). We therefore conclude, based on the microscopy, that the polycrystalline nature of the MOF thin film precludes long-range diffusion due to grain boundaries of crystalline grains smaller than the resolution limit of our microscope (≈140 nm). However, the microscopy confirms that efficient transport is present within the grains, as TTA significantly alters the shape of the observed PL spot. In order to directly observe micron-scale triplet transport, further strides must be taken to increase the size of the crystalline domains.

3. Conclusion

To conclude, we investigated the triplet excited energy transport of a surface-anchored metal-organic framework material based on an organic palladium-porphyrin linker. The highly

ordered MOF structure with close spacing between adjacent linker sheets facilitates highly efficient, one-dimensional triplet exciton transport between cofacial porphyrin units. Transient absorption measurements confirm one-dimensional transport of the triplet excitons with a transfer rate of 8×10^{10} s^{-1}. A theoretical analysis reveals strong π-π intermolecular interactions and substantial electronic coupling between the J-aggregated porphyrin linkers in one direction. These improve the Dexter exchange electronic coupling during the exciton transfer, and lead to a dominating influence of virtual (intermediate) charge transfer excitons. This has a strong impact on the theoretically obtained TEET rate (1×10^{10} s^{-1}), which we find in good agreement with the experimental value. From the photophysical parameters, we would expect exciton diffusion lengths on the order of several micrometers. From luminescence microscopy, however, we learned that for our current samples the diffusion length is restricted by the domain sizes of the polycrystalline PdP SURMOF films, but that strong TTA within domains occurs due to the excellent mobility of triplets within crystals and dictates the observed PL profiles. The excellent triplet transfer rates in these easily-deposited thin-film coatings create strong interest with regard to applications in light harvesting. Even though the PdP SURMOF forms stable photoproducts under extended illumination, their effect on the triplet population is small compared to the efficient TTA, which is enabled by the material's transport properties.[29] Moreover, the general concept of using long-lived triplet excitons to carry energy over large distances in a well-ordered SURMOF could be extended to more photostable molecules. Regardless, expanding the domain sizes will be necessary in order to realize large excitonic diffusion lengths. In this context we will investigate recently introduced variants of the layer-by-layer method to fabricate SURMOFs of reduced defect density, e.g. by using ultrasonication as an intermediate step.[60]

4. Experimental section

Materials

Zinc acetate and ethanol were purchased from VWR and used as received. The PdP linker was synthesized starting from 5,15-bis(4'-methoxycarbonyl)phenyl)-10,20-diphenylporphyrin.[61].

Sample preparation

The PdP SURMOFs were fabricated by spray coating using a zinc acetate solution in ethanol (1 mM L^{-1}) and a PdP linker solution in ethanol (20 μM L^{-1}). The zinc acetate solution was sprayed on the substrate (for 15 s), followed by a waiting time (35 s) and rinsing with pure ethanol (5 s). Then the linker solution was sprayed on top (25 s) followed by a waiting time (35 s) and rinsing with pure ethanol (5 s). These steps were repeated 15 or 30 times. The growth rate was previously determined to be around 16 nm per cycle[28]. Crystallinity of the thin film was ascertained by X-ray diffraction (XRD) characterization (Bruker D8 Advance).

Absorption spectroscopy

Absorption spectra were measured with a Perkin-Elmer Lambda 950 UV/vis/NIR spectrophotometer in absorbance mode. The PdP linker solution was measured in transmission mode with the cuvette placed in the beam path. The thin-film PdP SURMOF sample was measured inside an integrating sphere.

Steady-state photoluminescence spectroscopy

The sample was excited with a 525 nm continuous wave (CW) laser diode (Roithner LaserTechnik LD-515-10MG, tuned to 525 nm) and the emission spectra were measured with a fiber-coupled CCD spectrometer (Avantes AvaSpec ULS-RS-TEC). The sample was kept under dynamic vacuum ($<10^{-4}$ Pa).

Determination of the monomolecular lifetime

The sample was excited at 525 nm with a laser diode (Roithner LaserTechnik LD-515-10MG, tuned to 525 nm) modulated with square-wave pulses at 200 Hz (using a Thorlabs ITC4001 laser diode and TEC controller in QCW mode; 1 ms on, 4 ms off). The sample was kept under dynamic vacuum ($<10^{-4}$ Pa). The phosphorescence spectra were measured after a 550 nm longpass filter (Thorlabs FEL0550) using a double monochromator (Bentham DTMS300) and a photomultiplier tube (PMT, Hamamatsu R928P). The phosphorescence decay kinetics were obtained from the PMT signal using multi-channel-scaling electronics (PicoQuant TimeHarp 260 NANO). The resulting decay curve was fitted with a single exponential function to obtain the lifetime. The data are shown in Figure S1.

Transient absorption spectroscopy (TAS)

Nanosecond TAS was performed with a custom-built pump-probe system. The output of a titanium:sapphire (Ti:Sa) femtosecond amplifier (SpectraPhysics Spitfire Pro XP, center wavelength 800 nm, repetition rate 1kHz) was used to generate a white light continuum (probe beam) inside a sapphire crystal. The pump beam was generated from an oscillator/amplifier sub-nanosecond laser system (Innolas Picolo AOT 1 MOPA, center wavelength 532 nm, repetition rate 500 Hz, pulse width 800 ps). The pump laser was electronically triggered by the Ti:Sa amplifier, the pump-probe delay could be set by delaying this trigger signal using a digital delay generator (Stanford Research Systems DG535). To prevent triplet quenching by atmospheric oxygen, the sample was kept under dynamic vacuum with pressure less than 10^{-4} Pa. After passing the sample, the probe beam was dispersed on a flint glass prism and detected at 1 kHz on a linear image sensor (Hamamatsu NMOS S3904-512Q). Each probe pulse from the laser was read out into computer software and adjacent readings were used to calculate the transient absorption data $\Delta T/T$ (differential transmission).

Luminescence microscopy

The experiments were performed on a widefield inverted microscope (Zeiss Axio ObserverZ1, Jena, Germany) as previously described.[62] Briefly, a 405 nm laser (Stradus 405-250, Vortran Laser Technology, Sacramento, CA) beam was passed through an acousto-optical tunable filter (AOTF, model AOTFnC-400.650, A-A Opto-Electronic, Orsay, France) and coupled into a fiber for spatial filtering. The output of the fiber was collimated by a convex lens and focused by an oil immersion objective (Zeiss alpha Plan-Apochromat 63×/1.46 Oil Corr M27) into the sample. The phosphorescence signal or the scattered light from the excitation light

were collected by the same objective, passed through bandpass filters (FB405-10, 405/10 nm (center/FWHM), Thorlabs, Munich, Germany, for the excitation light; BrightLine HC 698/70, AHF, Tübingen, Germany, for phosphorescence) and imaged onto an EMCCD camera (Ixon Ultra X-7759, Andor, Belfast, UK). To prevent triplet quenching by atmospheric oxygen, the thin film PdP SURMOF sample was previously encapsulated under nitrogen atmosphere. A schematic drawing of the microscopy setup and a detailed description of the data analysis process can be found in the Supporting Information.

Quantum-chemical calculations

Microscopic parameters of PdP SURMOF were calculated using the dimer approach, where the two adjacent porphyrin linkers in the MOF intersheet direction were considered. The PdP dimer was taken from the GGA-optimized SURMOF using VASP,[63] v. 5.4.1 (computational details described in the Supporting Information). The corresponding PdP carboxylate groups were saturated with hydrogen atoms. The position of the PdP linkers, as known from the SURMOF structure, was kept by fixing the position of the oxygen atoms. The short-range electronic coupling matrix elements between the porphyrin linkers were calculated using the conventional and time-dependent density functional theory method, utilizing hybrid B3LYP[64], and hybrid long-range separated CAM-B3LYP[65] functionals with def2-SVP basis set[66,67] and Grimme D3 dispersion correction.[68] Both direct coupling and energy splitting method were used to calculate the electronic coupling elements during the TEET exciton transport in the PdP SURMOF. TEET coupling calculations were made with Turbomole[69] (V7.1 2016) and Gaussian 16,[70] as described in the Supporting Information.

ASSOCIATED CONTENT

Supporting Information. X-Ray Diffraction data; monomolecular triplet lifetime determination; calculation of triplet concentration from TAS kinetics and initial concentrations; fit of a 3D diffusion model to γ(t); discussion of the factor *f* in the rate equation; additional information on the acquisition, processing and analysis of the luminescence microscopy data; additional information on the theoretical calculations.

AUTHOR INFORMATION

Corresponding Author

Dr. Ian Howard, ian.howard@kit.edu

Author Contributions

M. A., B. S. R., and I. A. H. conceived and designed the experiments with assistance from C. W. on matters relating to the SURMOF fabrication and G. U. N. on matters relating to the microscopy measurements. The PdP linkers were designed and synthesized by G. E. and M. O. S.; N. B. and M. O. S. prepared the PdP SURMOF samples with the guidance of C. W. M. A. performed the absorption spectroscopy, TAS experiments, steady-state PL spectroscopy and the lifetime determination and analyzed the acquired data. D. B. and A. T. assisted with the optical measurements and SURMOF chemistry respectively. R. M. performed the microscopy experiments under the guidance of G. U. N, and M. A. analyzed the acquired data. M. K. performed and analyzed the quantum mechanical calculations. The paper was written by M. A., M. K. and I. A. H. and all authors discussed the results and commented on the paper.

Funding Sources

Helmholtz Association, Chinese Scholarship Council, Baden-Württemberg Stiftung, Science Foundation Ireland (IvP 13/IA/1894).

Notes

Any additional relevant notes should be placed here.

ACKNOWLEDGMENT

This work was supported by the Helmholtz Program Science and Technology of Nanosystems (STN) and the Helmholtz Energy Materials Foundry (HEMF). M. A. acknowledges support from Karlsruhe School of Optics and Photonics (KSOP) graduate school. R. M. acknowledges financial support by the Chinese Scholarship Council (CSC). I. A. H. and M.A. thank the Baden-Württemberg Stiftung for financial support. M. O. S. acknowledges grant support from the Science Foundation Ireland (IvP 13/IA/1894). B. S. R. would like to acknowledge the financial support provided by Helmholtz Recruitment Initiative Fellowship. M.K. acknowledges funding by M-ERA.NET MODIGLIANI and SFB 1176. M.K. is very grateful to F. Symalla, P. Friederich and S. Heidrich for fruitful discussions. Parts of this work were performed on the computational resource ForHLR II funded by the Ministry of Science, Research and the Arts Baden-Württemberg and DFG (“Deutsche Forschungsgemeinschaft”).

ABBREVIATIONS

MOF, Metal-Organic Framework;

SURMOF, Surface-Anchored Metal-Organic Framework;

PdP, (5,15-bis(4-carboxyphenyl)-10,20-diphenylporphyrinato)palladium(II);

PdTPP, (5,10,15,20-tetrakis(4-phenylethynyl)phenylporphyrinato)palladium(II);

TAS, Transient absorption spectroscopy;

TTA, triplet-triplet annihilation;

TEET, triplet exciton energy transfer;

DFT, density functional theory;

HOMO, highest occupied molecular orbital;

LUMO, lowest unoccupied molecular orbital;

CT, charge transfer;

CW, continuous wave;

PL, photoluminescence;

PLQY, photoluminescence quantum yield;

REFERENCES

(1) Eddaoudi, M.; Kim, J.; Rosi, N.; Vodak, D.; Wachter, J.; O'Keeffe, M.; Yaghi, O. M. Systematic Design of Pore Size and Functionality in Isoreticular MOFs and Their Application in Methane Storage. *Science* **2002**, *295* (5554), 469–472. https://doi.org/10.1126/science.1067208.

(2) Stassen, I.; Burtch, N.; Talin, A.; Falcaro, P.; Allendorf, M.; Ameloot, R. An Updated Roadmap for the Integration of Metal–Organic Frameworks with Electronic Devices and Chemical Sensors. *Chem. Soc. Rev.* **2017**, *46* (11), 3185–3241. https://doi.org/10.1039/C7CS00122C.

(3) Kim, S.; Joarder, B.; Hurd, J. A.; Zhang, J.; Dawson, K. W.; Gelfand, B. S.; Wong, N. E.; Shimizu, G. K. H. Achieving Superprotonic Conduction in Metal–Organic Frameworks through Iterative Design Advances. *J. Am. Chem. Soc.* **2018**, *140* (3), 1077–1082. https://doi.org/10.1021/jacs.7b11364.

(4) Sun, L.; Campbell, M. G.; Dincă, M. Electrically Conductive Porous Metal–Organic Frameworks. *Angew. Chem. Int. Ed.* **2016**, *55* (11), 3566–3579. https://doi.org/10.1002/anie.201506219.

(5) Cao, L.; Lin, Z.; Shi, W.; Wang, Z.; Zhang, C.; Hu, X.; Wang, C.; Lin, W. Exciton Migration and Amplified Quenching on Two-Dimensional Metal–Organic Layers. *J. Am. Chem. Soc.* **2017**, *139* (20), 7020–7029. https://doi.org/10.1021/jacs.7b02470.

(6) C. So, M.; P. Wiederrecht, G.; E. Mondloch, J.; T. Hupp, J.; K. Farha, O. Metal–Organic Framework Materials for Light-Harvesting and Energy Transfer. *Chem. Commun.* **2015**, *51* (17), 3501–3510. https://doi.org/10.1039/C4CC09596K.

(7) Liu, J.; Zhou, W.; Liu, J.; Howard, I.; Kilibarda, G.; Schlabach, S.; Coupry, D.; Addicoat, M.; Yoneda, S.; Tsutsui, Y.; et al. Photoinduced Charge-Carrier Generation in Epitaxial MOF Thin Films: High Efficiency as a Result of an Indirect Electronic Band Gap? *Angew. Chem. Int. Ed.* **2015**, *54* (22), 7441–7445. https://doi.org/10.1002/anie.201501862.

(8) Dolgopolova, E. A.; Rice, A. M.; Martin, C. R.; Shustova, N. B. Photochemistry and Photophysics of MOFs: Steps towards MOF-Based Sensing Enhancements. *Chem. Soc. Rev.* **2018**, *47* (13), 4710–4728. https://doi.org/10.1039/C7CS00861A.

(9) Kim, H.; Yang, S.; Rao, S. R.; Narayanan, S.; Kapustin, E. A.; Furukawa, H.; Umans, A. S.; Yaghi, O. M.; Wang, E. N. Water Harvesting from Air with Metal-Organic Frameworks Powered by Natural Sunlight. *Science* **2017**, *356* (6336), 430–434. https://doi.org/10.1126/science.aam8743.

(10) Lunt, R. R.; Benziger, J. B.; Forrest, S. R. Relationship between Crystalline Order and Exciton Diffusion Length in Molecular Organic Semiconductors. *Adv. Mater.* **2010**, *22* (11), 1233–1236. https://doi.org/10.1002/adma.200902827.

(11) Wan, Y.; Stradomska, A.; Knoester, J.; Huang, L. Direct Imaging of Exciton Transport in Tubular Porphyrin Aggregates by Ultrafast Microscopy. *J. Am. Chem. Soc.* **2017**, *139* (21), 7287–7293. https://doi.org/10.1021/jacs.7b01550.

(12) Haedler, A. T.; Kreger, K.; Issac, A.; Wittmann, B.; Kivala, M.; Hammer, N.; Köhler, J.; Schmidt, H.-W.; Hildner, R. Long-Range Energy Transport in Single Supramolecular Nanofibres at Room Temperature. *Nature* **2015**, *523* (7559), 196–199. https://doi.org/10.1038/nature14570.

(13) Dubin, F.; Melet, R.; Barisien, T.; Grousson, R.; Legrand, L.; Schott, M.; Voliotis, V. Macroscopic Coherence of a Single Exciton State in an Organic Quantum Wire. *Nat. Phys.* **2006**, *2* (1), 32–35. https://doi.org/10.1038/nphys196.
(14) Irkhin, P.; Biaggio, I. Direct Imaging of Anisotropic Exciton Diffusion and Triplet Diffusion Length in Rubrene Single Crystals. *Phys. Rev. Lett.* **2011**, *107* (1), 017402. https://doi.org/10.1103/PhysRevLett.107.017402.
(15) Liu, J.; Wöll, C. Surface-Supported Metal–Organic Framework Thin Films: Fabrication Methods, Applications, and Challenges. *Chem. Soc. Rev.* **2017**, *46* (19), 5730–5770. https://doi.org/10.1039/C7CS00315C.
(16) Zhang, Q.; Zhang, C.; Cao, L.; Wang, Z.; An, B.; Lin, Z.; Huang, R.; Zhang, Z.; Wang, C.; Lin, W. Förster Energy Transport in Metal–Organic Frameworks Is Beyond Step-by-Step Hopping. *J. Am. Chem. Soc.* **2016**, *138* (16), 5308–5315. https://doi.org/10.1021/jacs.6b01345.
(17) Son, H.-J.; Jin, S.; Patwardhan, S.; Wezenberg, S. J.; Jeong, N. C.; So, M.; Wilmer, C. E.; Sarjeant, A. A.; Schatz, G. C.; Snurr, R. Q.; et al. Light-Harvesting and Ultrafast Energy Migration in Porphyrin-Based Metal–Organic Frameworks. *J. Am. Chem. Soc.* **2013**, *135* (2), 862–869. https://doi.org/10.1021/ja310596a.
(18) Goswami, S.; Ma, L.; Martinson, A. B. F.; Wasielewski, M. R.; Farha, O. K.; Hupp, J. T. Toward Metal–Organic Framework-Based Solar Cells: Enhancing Directional Exciton Transport by Collapsing Three-Dimensional Film Structures. *ACS Appl. Mater. Interfaces* **2016**, *8* (45), 30863–30870. https://doi.org/10.1021/acsami.6b08552.
(19) Zhu, J.; Maza, W. A.; Morris, A. J. Light-Harvesting and Energy Transfer in Ruthenium(II)-Polypyridyl Doped Zirconium(IV) Metal-Organic Frameworks: A Look toward Solar Cell Applications. *J. Photochem. Photobiol. A: Chem.* **2017**, *344*, 64–77. https://doi.org/10.1016/j.jphotochem.2017.04.025.
(20) Williams, D. E.; Shustova, N. B. Metal–Organic Frameworks as a Versatile Tool To Study and Model Energy Transfer Processes. *Chem. Eur. J.* **2015**, *21* (44), 15474–15479. https://doi.org/10.1002/chem.201502334.
(21) Deria, P.; Yu, J.; Balaraman, R. P.; Mashni, J.; White, S. N. Topology-Dependent Emissive Properties of Zirconium-Based Porphyrin MOFs. *Chem. Commun.* **2016**, *52* (88), 13031–13034. https://doi.org/10.1039/C6CC07343C.
(22) Lee, C. Y.; Farha, O. K.; Hong, B. J.; Sarjeant, A. A.; Nguyen, S. T.; Hupp, J. T. Light-Harvesting Metal–Organic Frameworks (MOFs): Efficient Strut-to-Strut Energy Transfer in Bodipy and Porphyrin-Based MOFs. *J. Am. Chem. Soc.* **2011**, *133* (40), 15858–15861. https://doi.org/10.1021/ja206029a.
(23) Haldar, R.; Jakoby, M.; Mazel, A.; Zhang, Q.; Welle, A.; Mohamed, T.; Krolla, P.; Wenzel, W.; Diring, S.; Odobel, F.; et al. Anisotropic Energy Transfer in Crystalline Chromophore Assemblies. *Nat. Commun.* **2018**, *9* (1). https://doi.org/10.1038/s41467-018-06829-3.
(24) Park, K. C.; Seo, C.; Gupta, G.; Kim, J.; Lee, C. Y. Efficient Energy Transfer (EnT) in Pyrene- and Porphyrin-Based Mixed-Ligand Metal–Organic Frameworks. *ACS Appl. Mater. Interfaces* **2017**, *9* (44), 38670–38677. https://doi.org/10.1021/acsami.7b14135.
(25) Yu, J.; Park, J.; Van Wyk, A.; Rumbles, G.; Deria, P. Excited-State Electronic Properties in Zr-Based Metal–Organic Frameworks as a Function of a Topological Network. *J. Am. Chem. Soc.* **2018**, *140* (33), 10488–10496. https://doi.org/10.1021/jacs.8b04980.

(26) Yost, S. R.; Hontz, E.; Yeganeh, S.; Van Voorhis, T. Triplet vs Singlet Energy Transfer in Organic Semiconductors: The Tortoise and the Hare. *J. Phys. Chem. C* **2012**, *116* (33), 17369–17377. https://doi.org/10.1021/jp304433t.
(27) Lin, J.; Hu, X.; Zhang, P.; Van Rynbach, A.; Beratan, D. N.; Kent, C. A.; Mehl, B. P.; Papanikolas, J. M.; Meyer, T. J.; Lin, W.; et al. Triplet Excitation Energy Dynamics in Metal–Organic Frameworks. *J. Phys. Chem. C* **2013**, *117* (43), 22250–22259. https://doi.org/10.1021/jp401515r.
(28) Oldenburg, M.; Turshatov, A.; Busko, D.; Wollgarten, S.; Adams, M.; Baroni, N.; Welle, A.; Redel, E.; Wöll, C.; Richards, B. S.; et al. Photon Upconversion at Crystalline Organic–Organic Heterojunctions. *Adv. Mater.* **2016**, *28* (38), 8477–8482. https://doi.org/10.1002/adma.201601718.
(29) Adams, M.; Baroni, N.; Oldenburg, M.; Kraffert, F.; Behrends, J.; MacQueen, R. W.; Haldar, R.; Busko, D.; Turshatov, A.; Emandi, G.; et al. Reaction of Porphyrin-Based Surface-Anchored Metal–Organic Frameworks Caused by Prolonged Illumination. *Phys. Chem. Chem. Phys.* **2018**, *20* (46), 29142–29151. https://doi.org/10.1039/C8CP05254A.
(30) Liu, J.; Lukose, B.; Shekhah, O.; Arslan, H. K.; Weidler, P.; Gliemann, H.; Bräse, S.; Grosjean, S.; Godt, A.; Feng, X.; et al. A Novel Series of Isoreticular Metal Organic Frameworks: Realizing Metastable Structures by Liquid Phase Epitaxy. *Sci. Rep.* **2012**, *2*, 921. https://doi.org/10.1038/srep00921.
(31) Arslan, H. K.; Shekhah, O.; Wohlgemuth, J.; Franzreb, M.; Fischer, R. A.; Wöll, C. High-Throughput Fabrication of Uniform and Homogenous MOF Coatings. *Adv. Funct. Mater.* **2011**, *21* (22), 4228–4231. https://doi.org/10.1002/adfm.201101592.
(32) Verma, S.; Ghosh, H. N. Exciton Energy and Charge Transfer in Porphyrin Aggregate/Semiconductor (TiO2) Composites. *J. Phys. Chem. Lett.* **2012**, *3* (14), 1877–1884. https://doi.org/10.1021/jz300639q.
(33) Solov'ev, K. N.; Tsvirko, M. P.; Sapunov, V. V. Quantum Yield for Intersystem Crossing in Nonfluorescent Metal Porphyrins. *J. Appl. Spectrosc.* **1973**, *18* (4), 543–545. https://doi.org/10.1007/BF00604521.
(34) Önal, E.; Saß, S.; Hurpin, J.; Ertekin, K.; Topal, S. Z.; Kumke, M. U.; Hirel, C. Lifetime-Based Oxygen Sensing Properties of Palladium(II) and Platinum(II) Meso-Tetrakis(4-Phenylethynyl)Phenylporphyrin. *J. Fluoresc.* **2017**, *27* (3), 861–868. https://doi.org/10.1007/s10895-016-2022-x.
(35) Rogers, J. E.; Nguyen, K. A.; Hufnagle, D. C.; McLean, D. G.; Su, W.; Gossett, K. M.; Burke, A. R.; Vinogradov, S. A.; Pachter, R.; Fleitz, P. A. Observation and Interpretation of Annulated Porphyrins: Studies on the Photophysical Properties of Meso-Tetraphenylmetalloporphyrins. *J. Phys. Chem. A* **2003**, *107* (51), 11331–11339. https://doi.org/10.1021/jp0354705.
(36) Johnson, E. R.; Keinan, S.; Mori-Sánchez, P.; Contreras-García, J.; Cohen, A. J.; Yang, W. Revealing Noncovalent Interactions. *J. Am. Chem. Soc.* **2010**, *132* (18), 6498–6506. https://doi.org/10.1021/ja100936w.
(37) Chandrasekhar, S. Stochastic Problems in Physics and Astronomy. *Rev. Mod. Phys.* **1943**, *15* (1), 1–89. https://doi.org/10.1103/RevModPhys.15.1.
(38) Liu, C.; Tang, H.; Bard, A. J. Effect of Orientation of Porphyrin Single-Crystal Slices on Optoelectronic Properties. *J. Phys. Chem.* **1996**, *100* (9), 3587–3591. https://doi.org/10.1021/jp9516093.

(39) Lüer, L.; Hoseinkhani, S.; Polli, D.; Crochet, J.; Hertel, T.; Lanzani, G. Size and Mobility of Excitons in (6, 5) Carbon Nanotubes. *Nat. Phys.* **2009**, *5* (1), 54–58. https://doi.org/10.1038/nphys1149.
(40) Stehr, V.; Pfister, J.; Fink, R. F.; Engels, B.; Deibel, C. First-Principles Calculations of Anisotropic Charge-Carrier Mobilities in Organic Semiconductor Crystals. *Phys. Rev. B* **2011**, *83* (15), 155208. https://doi.org/10.1103/PhysRevB.83.155208.
(41) Fishchuk, I. I.; Kadashchuk, A.; Sudha Devi, L.; Heremans, P.; Bässler, H.; Köhler, A. Triplet Energy Transfer in Conjugated Polymers. II. A Polaron Theory Description Addressing the Influence of Disorder. *Phys. Rev. B* **2008**, *78* (4), 045211. https://doi.org/10.1103/PhysRevB.78.045211.
(42) Hibma, T.; Kommandeur, J. Dynamics of Triplet Excitons in the Simple Tetracyanoquinodimethane (TCNQ) Salts of Rubidium, Potassium, and Tri-Methyl-Benzimidazol. *Phys. Rev. B* **1975**, *12* (7), 2608–2618. https://doi.org/10.1103/PhysRevB.12.2608.
(43) Akselrod, G. M.; Deotare, P. B.; Thompson, N. J.; Lee, J.; Tisdale, W. A.; Baldo, M. A.; Menon, V. M.; Bulović, V. Visualization of Exciton Transport in Ordered and Disordered Molecular Solids. *Nat. Commun.* **2014**, *5*, 3646. https://doi.org/10.1038/ncomms4646.
(44) Lee, T. S.; Lin, Y. L.; Kim, H.; Pensack, R. D.; Rand, B. P.; Scholes, G. D. Triplet Energy Transfer Governs the Dissociation of the Correlated Triplet Pair in Exothermic Singlet Fission. *J. Phys. Chem. Lett.* **2018**, *9* (14), 4087–4095. https://doi.org/10.1021/acs.jpclett.8b01834.
(45) Van Wyk, A.; Smith, T.; Park, J.; Deria, P. Charge-Transfer within Zr-Based Metal–Organic Framework: The Role of Polar Node. *J. Am. Chem. Soc.* **2018**, *140* (8), 2756–2760. https://doi.org/10.1021/jacs.7b13211.
(46) Neumann, T.; Liu, J.; Wächter, T.; Friederich, P.; Symalla, F.; Welle, A.; Mugnaini, V.; Meded, V.; Zharnikov, M.; Wöll, C.; et al. Superexchange Charge Transport in Loaded Metal Organic Frameworks. *ACS Nano* **2016**, *10* (7), 7085–7093. https://doi.org/10.1021/acsnano.6b03226.
(47) Marcus, R. A. Electron Transfer Reactions in Chemistry. Theory and Experiment. *Reviews of Modern Physics* **1993**, *65* (3), 599–610. https://doi.org/10.1103/RevModPhys.65.599.
(48) Sudha Devi, L.; Al-Suti, M. K.; Dosche, C.; Khan, M. S.; Friend, R. H.; Köhler, A. Triplet Energy Transfer in Conjugated Polymers. I. Experimental Investigation of a Weakly Disordered Compound. *Phys. Rev. B* **2008**, *78* (4). https://doi.org/10.1103/PhysRevB.78.045210.
(49) Dexter, D. L. A Theory of Sensitized Luminescence in Solids. *J. Chem. Phys.* **1953**, *21* (5), 836–850. https://doi.org/10.1063/1.1699044.
(50) You, Z.-Q.; Hsu, C.-P. The Fragment Spin Difference Scheme for Triplet-Triplet Energy Transfer Coupling. *J. Chem. Phys.* **2010**, *133* (7), 074105. https://doi.org/10.1063/1.3467882.
(51) You, Z.-Q.; Hsu, C.-P. Theory and Calculation for the Electronic Coupling in Excitation Energy Transfer. *Int. J. Quant. Chem.* **2014**, *114* (2), 102–115. https://doi.org/10.1002/qua.24528.
(52) Hsu, C.-P. The Electronic Couplings in Electron Transfer and Excitation Energy Transfer. *Acc. Chem. Res.* **2009**, *42* (4), 509–518. https://doi.org/10.1021/ar800153f.

(53) Skourtis, S. S.; Liu, C.; Antoniou, P.; Virshup, A. M.; Beratan, D. N. Dexter Energy Transfer Pathways. *Proc. Natl. Acad. Sci. U.S.A.* **2016**, *113* (29), 8115–8120. https://doi.org/10.1073/pnas.1517189113.
(54) Wehner, J.; Baumeier, B. Intermolecular Singlet and Triplet Exciton Transfer Integrals from Many-Body Green's Functions Theory. *J. Chem. Theo. Comput.* **2017**, *13* (4), 1584–1594. https://doi.org/10.1021/acs.jctc.6b00935.
(55) Olaya-Castro, A.; Scholes, G. D. Energy Transfer from Förster–Dexter Theory to Quantum Coherent Light-Harvesting. *Int. Rev. Phys. Chem.* **2011**, *30* (1), 49–77. https://doi.org/10.1080/0144235X.2010.537060.
(56) Brédas, J.-L.; Beljonne, D.; Coropceanu, V.; Cornil, J. Charge-Transfer and Energy-Transfer Processes in π-Conjugated Oligomers and Polymers: A Molecular Picture. *Chem. Rev.* **2004**, *104* (11), 4971–5004. https://doi.org/10.1021/cr040084k.
(57) Aragó, J.; Troisi, A. Dynamics of the Excitonic Coupling in Organic Crystals. *Phys. Rev. Lett.* **2015**, *114* (2). https://doi.org/10.1103/PhysRevLett.114.026402.
(58) Bashir, A.; Heck, A.; Narita, A.; Feng, X.; Nefedov, A.; Rohwerder, M.; Müllen, K.; Elstner, M.; Wöll, C. Charge Carrier Mobilities in Organic Semiconductors: Crystal Engineering and the Importance of Molecular Contacts. *Phys. Chem. Chem. Phys.* **2015**, *17* (34), 21988–21996. https://doi.org/10.1039/C5CP03171K.
(59) Park, J.; Xu, M.; Li, F.; Zhou, H.-C. 3D Long-Range Triplet Migration in a Water-Stable Metal–Organic Framework for Upconversion-Based Ultralow-Power *in Vivo* Imaging. *J. Am. Chem. Soc.* **2018**, *140* (16), 5493–5499. https://doi.org/10.1021/jacs.8b01613.
(60) Müller, K.; Fink, K.; Schöttner, L.; Koenig, M.; Heinke, L.; Wöll, C. Defects as Color Centers: The Apparent Color of Metal–Organic Frameworks Containing Cu 2+-Based Paddle-Wheel Units. *ACS Appl. Mater. Interfaces* **2017**, *9* (42), 37463–37467. https://doi.org/10.1021/acsami.7b12045.
(61) Bakar, M. B.; Oelgemöller, M.; Senge, M. O. Lead Structures for Applications in Photodynamic Therapy. Part 2: Synthetic Studies for Photo-Triggered Release Systems of Bioconjugate Porphyrin Photosensitizers. *Tetrahedron* **2009**, *65* (34), 7064–7078. https://doi.org/10.1016/j.tet.2009.06.037.
(62) Li, Y.; Shang, L.; Nienhaus, G. U. Super-Resolution Imaging-Based Single Particle Tracking Reveals Dynamics of Nanoparticle Internalization by Live Cells. *Nanoscale* **2016**, *8* (14), 7423–7429. https://doi.org/10.1039/C6NR01495J.
(63) Kresse, G.; Hafner, J. Ab Initio Molecular Dynamics for Liquid Metals. *Phys. Rev. B* **1993**, *47* (1), 558–561. https://doi.org/10.1103/PhysRevB.47.558.
(64) Becke, A. D. Density-functional Thermochemistry. I. The Effect of the Exchange-only Gradient Correction. *J. Chem. Phys.* **1992**, *96* (3), 2155–2160. https://doi.org/10.1063/1.462066.
(65) Yanai, T.; Tew, D. P.; Handy, N. C. A New Hybrid Exchange–Correlation Functional Using the Coulomb-Attenuating Method (CAM-B3LYP). *Chem. Phys. Lett.* **2004**, *393* (1), 51–57. https://doi.org/10.1016/j.cplett.2004.06.011.
(66) Weigend, F.; Ahlrichs, R. Balanced Basis Sets of Split Valence, Triple Zeta Valence and Quadruple Zeta Valence Quality for H to Rn: Design and Assessment of Accuracy. *Phys. Chem. Chem. Phys.* **2005**, *7* (18), 3297–3305. https://doi.org/10.1039/B508541A.
(67) Schäfer, A.; Horn, H.; Ahlrichs, R. Fully Optimized Contracted Gaussian Basis Sets for Atoms Li to Kr. *J. Chem. Phys.* **1992**, *97* (4), 2571–2577. https://doi.org/10.1063/1.463096.

(68) Grimme, S.; Antony, J.; Ehrlich, S.; Krieg, H. A Consistent and Accurate Ab Initio Parametrization of Density Functional Dispersion Correction (DFT-D) for the 94 Elements H-Pu. *J. Chem. Phys.* **2010**, *132* (15), 154104. https://doi.org/10.1063/1.3382344.
(69) Ahlrichs, R.; Bär, M.; Häser, M.; Horn, H.; Kölmel, C. Electronic Structure Calculations on Workstation Computers: The Program System Turbomole. *Chem. Phys. Lett.* **1989**, *162* (3), 165–169. https://doi.org/10.1016/0009-2614(89)85118-8.
(70) Frisch, M. J.; Trucks, G. W.; Schlegel, H. B.; Scuseria, G. E.; Robb, M. A.; Cheeseman, J. R.; Scalmani, G.; Barone, V.; Petersson, G. A.; Nakatsuji, H.; et al. *Gaussian 16 Revision A.03*; 2016.